Journal of Materials and Engineering Structures

RETRACTED

Research Paper

Elastic-plastic analysis of reinforced composite materials

Mohamed Rida Seba [1], Said Kebdani [1], Ahmed Sahli [1,2], Sara Sahli [3]

[1] *Laboratoire de Mécanique Appliquée, Université des Sciences et de la Technologie d'Oran (USTO-MB), Algeria*

[2] *Laboratoire de recherche des technologies industrielles, Université Ibn Khaldoun de Tiaret, Algeria*

[3] *Université d'Oran 1 Ahmed Ben Bella, Algeria*

ARTICLE INFO

Article history :

Received : 11 October 2017

Revised : 6 December 2017

Accepted : 6 December 2017

Keywords:

Composite materials

Positional finite element method

Reinforced mediums

Associative plasticity

ABSTRACT

The paper deals with the implementation of two dimensional modelling solid elements with the discretization of the reinforcement, both of which can be analyzed in a plastic regime. Thus, ensuring a better representation of the real problem of a reinforced structure since some techniques use the homogenization of the section. The discretization of the reinforcement allows to treat this as a separate element and to study its interaction with the structure. In addition, it dispenses the constant generation of meshes with the formulation used. With the adopted formulations, the present work aims to study the behaviour of reinforced structures and the distribution of the reinforcement in the medium, in a random or aligned way. Considering the elastoplastic behavior of both, and evaluating the loss of rigidity of the structures, together with redistribution of efforts and, in some cases, the loss of instability by formation of plastic hinges and the interaction between the elements. The constitutive model for the plasticity adopted is the von Mises 2D associative with a positive linear hardening. The solution of this model was obtained through an iterative procedure. With the aim to ensure the correct implementation of the considered formulations, examples for validation and presentation of the functionalities of the developed computational code were analyzed.

1 Introduction

A composite material is the result of the macroscopic combination between two or more materials, in which the different phases can be seen with the naked eye. The advantage of composite materials is that, if well designed, they usually exhibit the best qualities of their components or constituents and often some qualities that neither constituent possesses [1].

The properties of a composite material depend on the properties of the constituents, their geometry, and the distribution of the phases. One of the most important parameters is the volume (or weight) fraction of reinforcement or fiber volume ratio [2].

* *Corresponding author. Tel.: +213 00000000.*
E-mail address: sebamr_2016@yahoo.com

e-ISSN: 2170-127X,

RESEARCH REVIEW of Sciences and Technologies

When the matrix is associated with fibers, there is a specific type of composite, referred to as a fiber-reinforced composite. An example of this class of composites is fiber reinforced concrete. Depending on the volumetric fraction of fibers, they play a different function in the set. When the fraction is less than 1%, the fibers have the reduction function of cracking by retraction. Fractions between 1% and 2% increase the modulus of rupture, hardness to fracture and impact strength. Beyond 2% increases the stiffness of the composite. Concretes that fit this condition are often called concretes reinforced with high performance fibers [3].

In order to make good use of the materials in engineering, understanding and predicting the behavior of the composite material in the short and long term should be possible. The main difficulty in dealing with composite materials is due to the great quantity of existing types of materials, and it is necessary to study each class. As it is possible to predict the behavior of a given composite by means of a numerical modelling, then it would be possible to have confidence that the projected material will meet the requirements by which it was designed [4].

According to Vanalli [5], the importance of a good representation of fiber-reinforced media in engineering analysis can be identified when a large number of papers are related to the evaluation of the behavior of this type of material and several alternatives present in commercial software and scientific articles for the Solution to this problem.

Gomes and Awruch [6] mention that in the last decades, several models for reinforced concrete have appeared to represent the behavior of the material up to a limit point, given by the state of [illegible] or last state. They presented satisfactory results for the needs they were designed for. For post-peak situations, displacement control techniques are commonly used, since the control of forces is not able to represent this behavior when Newton-Raphson is used.

There are three methods in the literature for the consideration of reinforcement in the set: homogenization, discretization and embedding. Homogenization is most appropriate for surface structures such as shells and plaques, which allow modelling of the reinforcement as a membrane layer within the cross section. For non-uniformly distributed reinforcement situations, the discretization and embedding techniques are more appropriate. However, it is common in discretization techniques to depend on the location of the reinforcement mesh with the matrix mesh, occurring the difficulty of generating the mesh of the reinforcement, and there may even be a constant process of generation of these until this condition is satisfied. This problem is even mor[illegible]l in three-dimensional cases [7].

In the present work, the finite element formulation used is positional, introduced by the works of [8, 9]. For this purpose, the positions are used as nodal parameters, differing initially from the classic approach by displacements, which greatly facilitates the consideration of the geometric non-linearity of the structure. Through a Total Lagrangian description, where the adopted reference configuration is the initial configuration, the equilibrium of the system is established at the current position, resulting in non-linear equations. For the resolution of these, Newton-Raphson's incremental-iterative method is used. The use of the Green-Lagrange objective deformation measure is also adopted; whose energetic conjugate is the tensor of Piola-Kirchhoff of the second species, in the description of the kinematics of the bodies.

For the insertion of reinforcement in the medium, the formulation used is proposed by [10] and found in works such as [5, 11]. This technique consists of contributing the effects of the fiber to the finite element representing the matrix, without increasing the number of degrees of freedom or the need for coincidence between the nodes of the finite elements of the reinforcement and the matrix. However, this method does not allow evaluating the sliding of the fiber, which is considered perfectly adherent.

Depending on the type of fiber and the interface between the fiber and the matrix, the following failure modes may occur: the crack develops and the fiber is stripped from the matrix, the matrix rupturing occurs, or the cracks propagate but are controlled Fibers [12].

Some mechanisms are used to evaluate the fiber rupture or the sliding of the matrix through the evaluation of the normal tension of the fiber and the shear stress of the interface between the fiber and the matrix, estimating forces to evaluate the governing plastification mechanism.

With the adopted formulations, the present work aims to study the behavior of reinforced structures, the distribution of the reinforcement in the medium, in a random or aligned way. Considering the elastoplastic behavior of both, it allows evaluating the loss of rigidity of the structures, together with redistribution of efforts and, in some cases, the loss of instability by formation of plastic hinges and the interaction between the elements.

The present work utilizes formulations that allow the representation of the fiber reinforced composite without the need of mesh coincidence. It also enables the simulation of the medium and the reinforcement at the elastoplastic regime, with the objective study better the real behaviour.

2 Finite element of bar as reinforcement

The formulations described in this chapter consist of simulating the fibers as a finite element of bar, having as nodal parameters the positions in each direction. The fibers are considered through two formulations. The first one considers the fibers as perfectly adhered to the medium [5, 10]. The second refer to the calculation of the internal and Hessian forces of the fibers, and the only difference between these topics is the degree of approximation of the element. The first item deals with fiber with only two nodes (linear approximation), and the second with a more general rule valid for any degree of approximation of fiber.

After the calculations of the internal and Hessian forces, the technique presented is used for the contribution of the fibers to the medium. This eliminates the coincidence of the nodes of the fiber mesh with the matrix mesh, considering the fibers as perfectly adhered to the medium and does not add degrees of freedom to the system.

2.1 Kinematics of straight Fiber Element

Figure 1 represents the different configurations that a finite element with linear approximation and its nodes can assume, and their relations with the auxiliary dimensionless configuration:

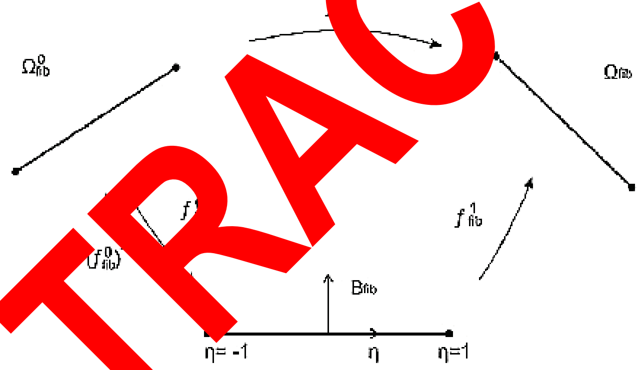

Fig. 1 - Schematic mapping of the straight fiber element and its initial and current configurations

Any point of the initial or undeformed configuration Ω^0_{fib} presents the x_i^{fib} coordinates in the Euclidean space, being mapped through the auxiliary dimensionless configuration B_{fib} with coordinate η ranging from -1 to 1, using functions of form ϕ_n^{fib} for interpolation through the positions of nodes of the finite element, $X_i^{n,fib}$. The index $i=1,2$ being the directions, fib the reference to the fiber element and the index n the number of nodes, in the case of the straight fiber equals two. Therefore, we have:

$$x_i^{fib} = \phi_n^{fib}(\eta) X_i^{n,fib} \tag{1}$$

For the current or deformed configuration Ω_{fib}, the coordinates y_i^{fib} of any point are mapped through the auxiliary dimensionless space with the current nodal positions $Y_i^{n,fib}$ as:

$$y_i^{fib} = \phi_n^{fib}(\eta) Y_i^{n,fib} \tag{2}$$

The function change of configuration $\overline{f}^{fib}$ is the one who makes the transition from the initial configuration to the final configuration, that is, that maps the coordinates x_i^{fib} to y_i^{fib}. Similar to the element of plate, this function can be obtained according to a composition between the mappings of the two configurations in relation to the dimensionless reference configuration as follows:

$$\overline{f}^{fib} = \overline{f}^{1,fib} \circ \left(\overline{f}^{0,fib}\right)^{-1} \tag{3}$$

3 Plasticity

The present topic and its considerations about the elastoplastic behavior of the structure and its constituent materials are widely discussed in the literature and can be found for example in [13-16]. The focus will be given to the importance of the study of plasticity and its differences in elastic behavior.

The plasticity is an observable phenomenon during the study of the materials microstructure, which indicates that the physical mechanism responsible for plasticity is the irreversible movement in defects in the atomic bonds, although there is no loss of cohesion or ruptures in the bonds. However, hardening may occur, due to incompatibilities between the deformations of the grains of the crystalline lattice [16]. Still according to [16], the elasticity is related to the complete disappearance of the structure deformations after the withdrawal of the force, that is, the deformations are reversible and are maintained only while the loading is applied. There is also viscoelasticity, which exhibits reversible but time-dependent deformations, which increase with time after application of the charge and decrease slowly after discharging.

The emergence of permanent deformations from energy dissipation is characteristic of plasticity, being an irreversible process. The recovery of the deformations after unloading is partial. This phenomenon of residual deformation becomes more evident in loading and unloading cycles. During unloading in the plastic regime, the slope is the same as loading and unloading under the elastic regime.

Elastoplastic behavior is of interest in terms of the resilient capacity of a structure. This is because although the calculations and details of some usual structures do not allow them to behave plastically and should be limited to the elastic regime, their disregard results in a waste of the additional resistance capacity that the plastic regime possesses.

4 Numerical treatment

In this section, seven examples are presented, aiming the validation of the developments and implementations presented in this paper. In all the examples, the plate elements used are triangular with cubic approximation and the ones of fiber present linear approximation. For the examples dealing with perfect elastoplasticity, a nearly zero tangent modulus was adopted, given the need for a non-zero tangent for Newton-Raphson's convergence in case of force control, not displacement.

4.1 Cantilever beam – large displacements

This example was developed with the purpose of validating the correct implementation of the positional formulation, which contemplates the effects of geometric nonlinearity. The results are compared with analytical results obtained in [17], in which elliptic integrals were used in the developments. The following hypotheses were adopted in the mentioned work: the material was considered linear elastic, deformations were ignored for axial effort and shear, the limbs were initially considered straight and with constant section, and the loading plane coincides with the plane of flexion.

[17] Related the dimensionless quantities u / L and w / L with another given by PL^2 / EI for a free and crimped beam subjected to a load at the free end, as shown in Figure 2. Being u the horizontal displacement, w the vertical displacement, P for the applied load, L the beam length, E the modulus of elasticity and I the moment of inertia.

For the present example, elastic modulus E = 3.10^5 KN/m^2 and a mesh with 448 triangular elements and 2176 degrees of freedom were distributed, as shown in the scheme of Figure 3.

In Figure 4, a comparison between the results of horizontal and vertical displacement obtained in [17] (analytical) and in the present work, for different levels of loading. It can be seen, the results compare very well, confirming the good behavior of the positional formulation.

In addition to the results of the present study, [17] showed that the maximum variation between the results is small and negligible. This discrepancy can be due to the conditions of loading and binding, since the finite element of [17] is one-dimensional beam and the present two-dimensional plate work.

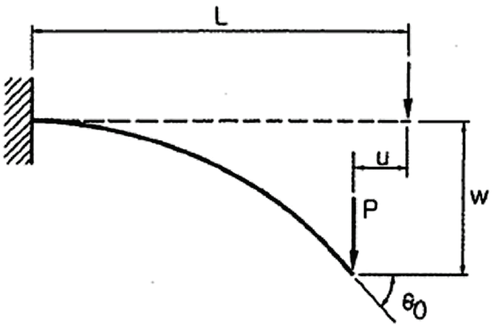

Fig. 2 - Fixed and horizontal free beam subjected to vertical loading

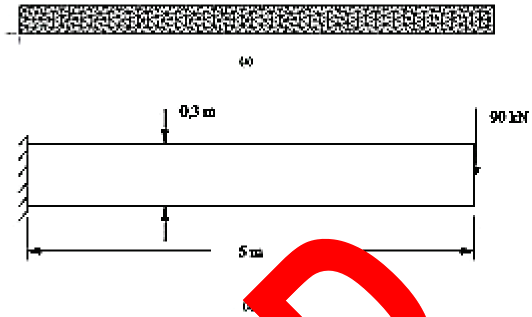

Fig. 3 - (a) Finite Element scheme (b) structure and boundary conditions and loading

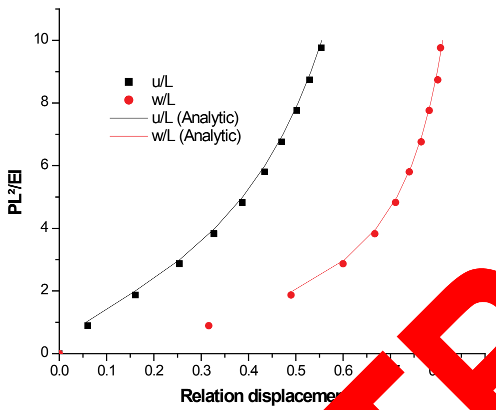

Fig. 4 - Comparative results for the Cantilever Beam free

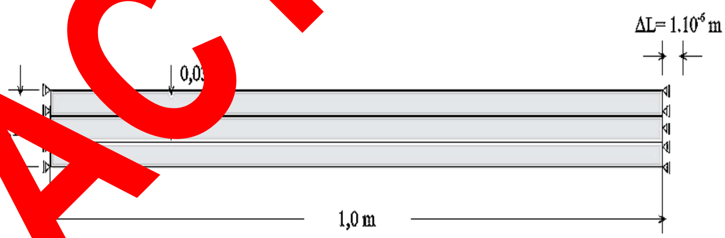

Fig. 5 - Reinforced bar subjected to tensile stress

The present formulation is still able to measure the geometric nonlinearity in high beams, because it is a finite element of plate, whereas the finite element of beam is only able to adequately represent long beams, that is, they have a height of section in relation to length.

4.2 Comparison with the Material Resistance technical solution

To verify the correct implementation of the formulation with the consideration of fiber reinforcement, the technical solution obtained from the Strength of Materials is used, in which the following hypotheses are made: homogeneous, isotropic, continuous, cohesive and linear materials.

Figure 5 shows the schematic referring to the structure and displacements prescribed: applied at the right tip of the structure:

The matrix has a thickness of e = 0,1m; ν = 0, modulus of elasticity $E_b = 2.10^{11}$ kN/m². Each reinforcement has an area equal to $A_r = 2.65.10^{-4}$ m² and modulus of elasticity $E_r = 3.10^{12}$ kN/m².

As the materials are consolidated, the reinforcements present the same displacement, which, according to the classical theory, can be related to the acting tension, thus:

$$\Delta L = \frac{PL}{E_r A_r} \quad \rightarrow \quad \sigma_r = \frac{\Delta L E_r}{L}$$

Substituting the values adopted, we have the classical theory:

$$\sigma_r = 3.10^6 \, kN / m^2$$

For the solution by the finite element method, 10 finite elements of single bar were used to simulate the reinforcements and 70 triangular plate elements. The prescribed displacements were applied directly to the nodes of the plate metal mesh. The result is shown in Figure 6.

As the prescribed displacements were applied directly to the nodes of the sheet mesh and not to reinforcement, together with the fact that there was no difference between the values obtained for the stresses by the positional finite element method and the classical theory, it can be concluded that Implementation of the formulation is correct. Considering also the same structure under the same bonding and displacement conditions, considering a reinforcement rupture stress as $\sigma_R = 2{,}01.10^6 \, kN / m^2$, the structure displacement analysis is performed after this tension, totally disregarding contribution of the reinforcement after it reaches the breaking stress level.

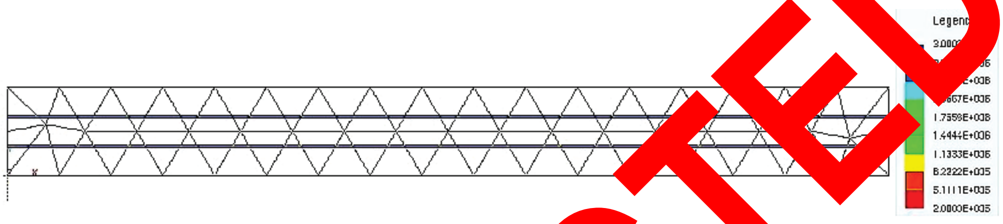

Fig. 6 - Reinforcement stress by the finite element method

As the stress distribution in the reinforcement is constant along the entire length, all elements failed at the same moment of displacement. When breaking, the elements fail to contribute to the rigidity of the system, and they should then have reaction values equal to the situation of the plate without reinforcement from this point, as shown in the result obtained in Figure 7.

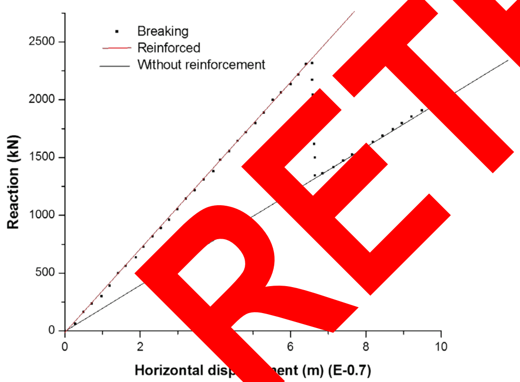

Fig. 7 - Load step x horizontal displacement

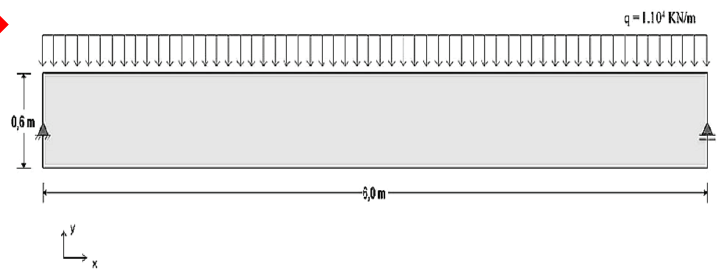

Fig. 8 - Bi-supported beam subjected to bending

4.3 Elastoplastic bi-supported beam subjected to uniformly distributed loading

To verify the correct implementation of plasticity in the matrix, a comparison of the results between the present formulation and commercial Ansys software was made.

Given the structure in Figure 8: for the material of the beam, the plastification stress $\sigma_Y = 3.10^6 \, kN / m^2$, the modulus of elasticity $E = 2.10^{11} \, kN / m^2$ and the tangent modulus $W = 5.10^{10} \, kN / m^2$.

For this example, a mesh with 940 elements and 8834 degrees of freedom was used. For Ansys, approximately 1300 elements with quadratic approximation were used. Figure 9, Figure 10 and Figure 11 present a comparison of the obtained results, for the lower face of the center of the span, in the present work and using the Ansys program, respectively, of displacement in the direction y, normal tension in the direction x and plastic deformation in the x direction. The results compare well with numerical solution:

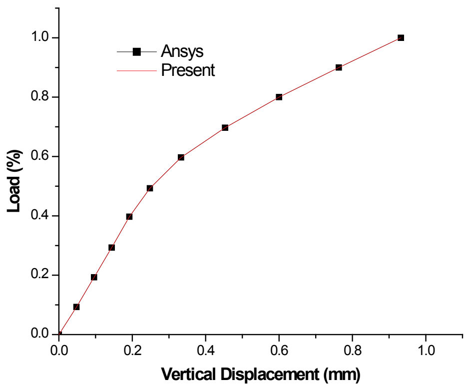

Fig. 9 - Comparison between the values of values x-direction

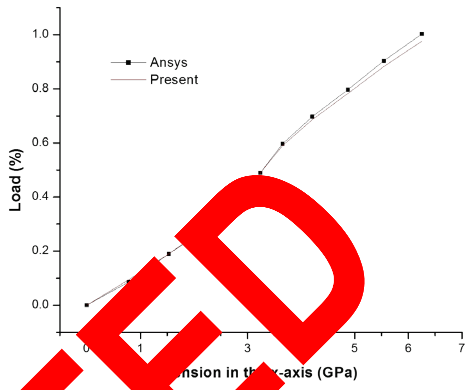

Fig. 10 - Comparison between stresses vertical displacements (y-axis)

It is possible to observe that the results show the same behavioural trends when entering the plastic regime, as well as the loading intensity for which the plastification process is initiated. In the final values obtained in the Ansys and in the present work, the percentage variations were 0.4% for the vertical displacement; 4.7% for the tension on the x-axis and 2.5% for the plastic deformation. Analyzing the obtained results, it can be concluded that the plasticity in the matrix was implemented correctly.

4.4 Moment of plastification in crimped-free beam

Given the example shown by [13] according to Figure 12, where the normal stress is completely redistributed in the section with a constant value equal to σ_Y, it is possible to calculate the plastification moment associated with the torque of the resulting forces in the section:

$$M_p = \sigma_Y h^2 b$$

Being h the [illegible] of the height of the section and b the width of the cross section of the beam, similar to the scheme of Figure 12. By adopting a plastification stress $\sigma_Y = 3.10^3\ kN/m^2$ and h = *0.2 m,* section width b = *0.1 m*, it is possible to conclude that the plastification moment for the adopted section is $M_p = 12\ kN.m$.

The plastification moment is always the same for the same section with the same properties; however, the value of the load applied at the free end of the beam that always generates the same moment value in the crimping depends on the length of the beam. Adopting three beams with the adopted section, but with lengths of 3 m, 4 m and 5 m; the applied concentrated loads associated with the plastification moment are 4 kN, 3 kN and 2,4 kN respectively. However, the loads were uniformly distributed at the free end of the beam, corresponding to the loads distributed at the height with a value of 10 kN/m, 7.5 kN/m and 6 kN/m, according to the basic scheme of Figure 13.

For the structure with spans of 3m, 4m and 5m were used meshes with, respectively, 1290 triangular elements and 12002 degrees of freedom, 1372 triangular elements and 12788 degrees of freedom, 1262 triangular elements and 11828 degrees of freedom. Figure 14 shows the graph of the applied force x vertical displacement ratio at the free end of the beam for the different length values adopted.

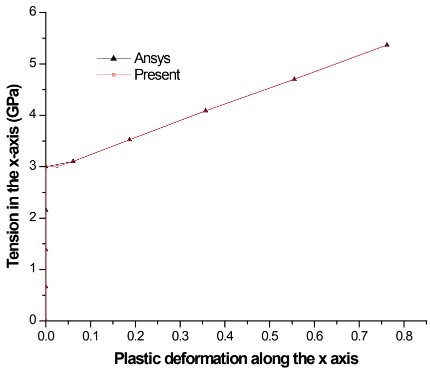

Fig. 11 - Comparison between the values of plastic deformation in the x direction

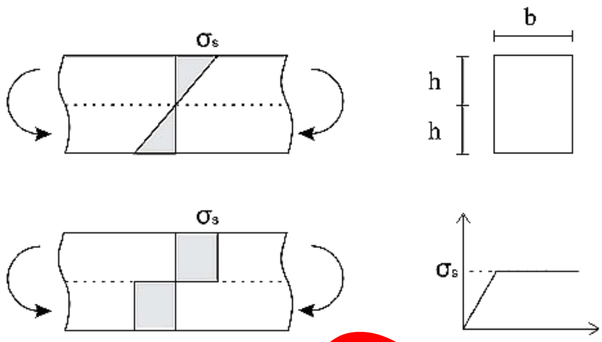

Fig. 12 - Elastic behavior vs plastic behavior of a beam (Adapted from [51])

Where σ_s is the stress that limits the elastic regime.

It is possible to observe that there was agreement between the theoretical loads for the plastization of the section of the beam and the perfect elastoplastic behavior according to the present formulation for the loads applied in the different beam lengths. In this way, it is possible to conclude that the perfect elastoplastic character was satisfactorily achieved for the representation of the loss of structure instability by the formation of the plastic kneecap in the crimping.

Figure 15 shows the stress distribution on the x-axis along the beam, while Figure 16 shows the plastic deformation on the x-axis. As shown in Figure 15, it is possible to observe that the tension is reaching the plastification value, even close to the middle of the section and that this results in the formation of the plastic ball joint next to the crimping, as shown in Figure 16, thus resulting in system instability.

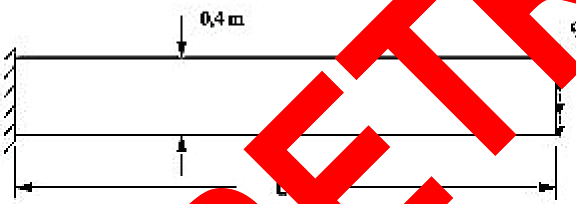

Fig. 13 - Structure diagram

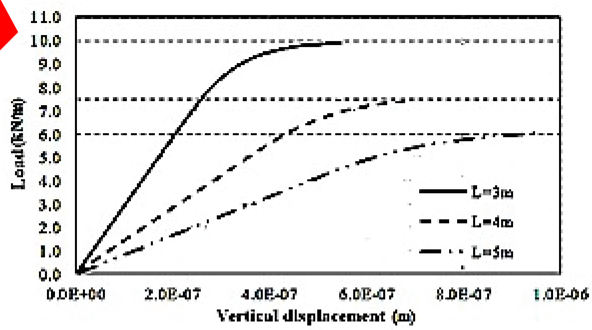

Fig. 14 - Graph (load x deformation) on beams of different lengths

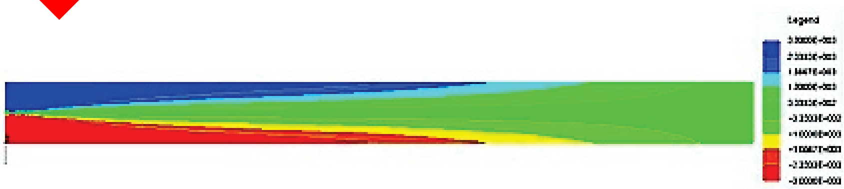

Fig. 15 - Tension distribution in the perfect elastoplastic matrix.

Fig. 16 - Distribution of the equivalent plastic deformation in the perfect elastoplastic matrix.

4.5 Plasticity in reinforcement

In this example, when using the same structure and conditions of linkage and displacements of example 4.2, it is desired to evaluate the implemented formulation with regard to plasticity in reinforcement. Assigning a near zero tangent modulus and setting the plastification stress of the reinforcement as the half of the tension in the last step of the elastic case of example 4.2, that is, $S_Y = 1,5.10^6\ kN/m^2$, the result in Figure 17 was obtained for the normal stress in the reinforcement according to the applied displacement level.

By analyzing the obtained graph, it is possible to verify the consistency of the results, because when fixing the plastification tension as half of the tension obtained in the last step for the elastic case, the plastification should occur in the middle of the loading steps. Also, since the elastoplastic model adopted was the perfect one, the tension level must remain constant, even if the prescribed displacement value is increased.

4.6 Analysis of the governing plasticity mechanism for the fibers

The present example is inspired by the one realized by [18], which aims to analyze the behavior of a structure with perfectly adhered fibers arranged randomly and to verify the governing mechanism of the plastification, either by normal stress in the fiber or shear at the interface.

Figure 18 illustrates the structure adopted and its boundary conditions and applied loads.

To evaluate the different plastification mechanisms, two types of fiber with the same physical properties, but with lengths *L= 3 cm and 6 cm* were chosen. Both have modulus of elasticity $E_{fib} = 2,1.10^7\ kN/cm^2$, area $A_r = 1\ cm^2$ and perimeter $\rho = 2\ cm$.

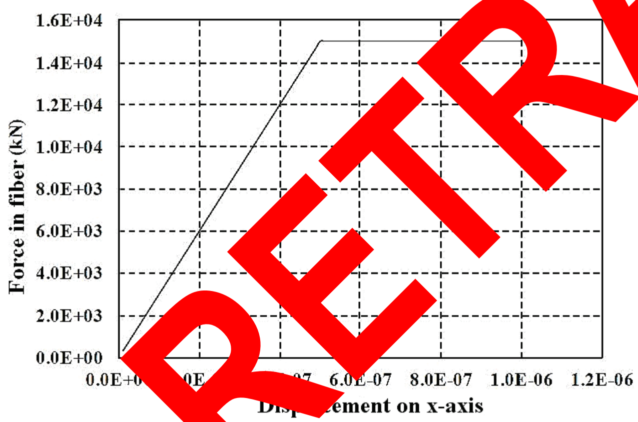

Fig. 17 – displacement and load diagram

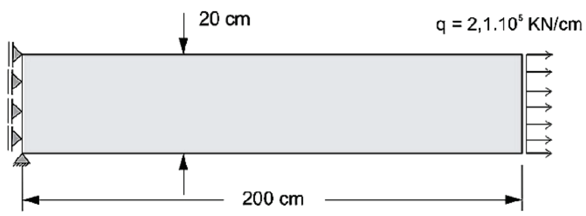

Fig. 18 - Schematic of the drawn plate

Adopting that the plastification tension for the fiber-matrix interface is $\tau_{plast} = 6.10^4\ kN/cm^2$ and the normal plastification tension in the perfectly adhered fiber is $\sigma_{plast} = 2.10^5\, kN/cm^2$, different mechanisms govern the plastification for each fiber length, according to the implemented formulation. For both, almost null tangent modulus was adopted. Applying the values adopted for the equations, we have:

For 3 cm fibers	**For 6 cm fibers**
$\bar{N}_1 \le \sigma_{adm} A \Rightarrow \bar{N}_1 = 2.10^5.1 = 2.10^5\ kN$	$\bar{N}_1 \le \sigma_{adm} A \Rightarrow \bar{N}_1 = 2.10^5.1 = 2.10^5\ kN$
$\bar{N}_2 \le \tau_{adm} \frac{l}{2} \rho_{fib} \Rightarrow \bar{N}_2 = 6.10^4.\left(\frac{3}{2}\right).2 = 1,8.10^5\ kN$	$\bar{N}_2 \le \tau_{adm} \frac{l}{2} \rho_{fib} \Rightarrow \bar{N}_2 = 6.10^4.\left(\frac{6}{2}\right).2 = 3,6.10^5\ kN$

In both cases, a fiber volume fraction of 50% was used in relation to the structure. For the situation of the fibers with length of 3cm, the force associated with the plastification of the fiber is $\bar{N}_1 = 2.10^5\ kN$ and for the plastification of the interface is $\bar{N}_2 = 1,8.10^5\ kN$, and therefore, the plastification occurs according to the strain-strain curve of the interface. For the situation of the fibers with a length of 6 cm, the force associated with the plastification of the fiber is $\bar{N}_1 = 2.10^5\ kN$ and for the plastification of the interface is $\bar{N}_2 = 3,6.10^5\ kN$, and therefore, the plastification occurs according to the strain-strain curve of the Normal fiber stress.

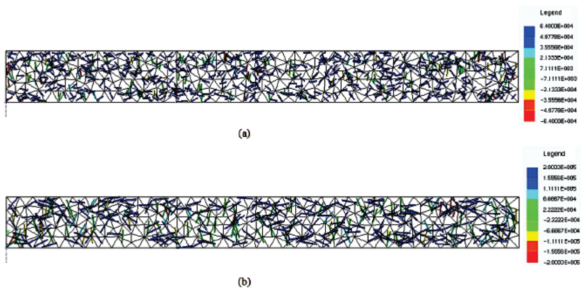

Fig. 19 - (a) normal tension in the elastoplastic fibers of 3cm, (b) normal tension in the elastoplastic fibers of 6cm

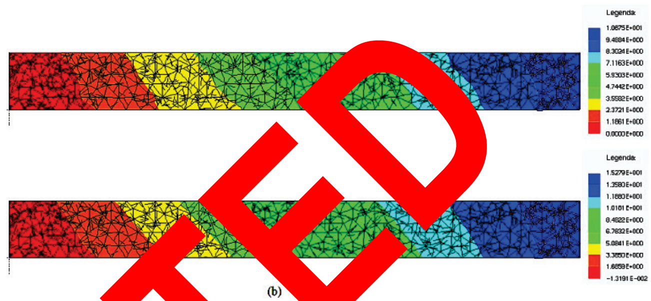

Fig. 20 - (a) horizontal displacements with elastic fibers, (b) horizontal displacements with plastic fibers

Figure 19 shows the tensions in the fibers for the cases of fibers with lengths of 3 cm and 6 cm, respectively:

Figure 20 shows the horizontal displacements in the matrix with the consideration of fibers, 3cm in length, elastic and elastoplastic, respectively; and in an analogous way, Figure 21 shows the horizontal displacements for the 6cm long fiber.

Analyzing the results of Figure 20 and Figure 21, it is possible to observe that, for the same case of fiber, the horizontal displacements were greater when the elastoplastic behavior of the fibers was considered and the distribution of horizontal displacement was smoother. This is due to the fact that the fibers considered as perfect elastoplastic only contribute in the rigidity until the plastification tension, whereas those considered elastic continue to concentrate tensions in the levels of greater loads.

By comparing the cases of 3cm fibers with those of 6cm in Figure 19, it is possible to visualize that the smaller fibers had larger displacements. This occurs because they are plasticized by the criterion of the interface tension, which has a lower plasticization tension to that of the fiber, thus less stiffening the medium than in the case where the plasticized fibers are at the criterion of the normal effort. It is also possible to observe, as shown in Figure 19, that the tensions in the elastoplastic fibers of both cases present values around the plastification stress according to each strain-strain curve.

4.7 Perfect elastoplasticity in reinforced crimped-free beam

This example aims to present the potentialities of the obtained formulation with respect to the consideration of the elastoplastic behavior for both the matrix and the fibers. For the present example, we consider a beam of length $L = 4\ m$, the half-height value $h = 0.2\ m$ and width of the unitary section, plastification stress of the matrix material $S_Y = 3.10^3\ kN/m^2$ and a prescribed displacement at the free end, as Shown in the scheme of Figure 22.

The prescribed displacement used has its value sufficient to form the plastic kneecap in the structure without the reinforcement, as shown in Figure 23. However, it is possible to observe that this does not occur with consideration of the elastic reinforcement in Figure 24.

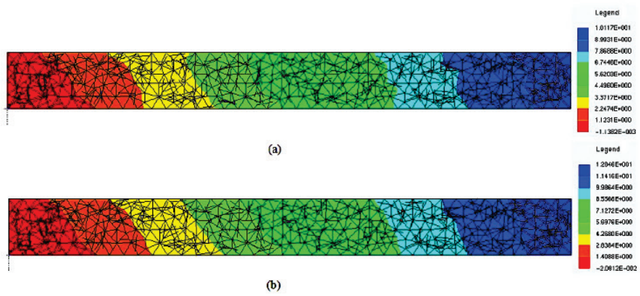

Fig. 21 - (a) horizontal displacements with elastic fibers, (b) horizontal displacements with plastic fibers

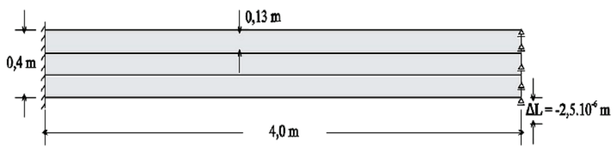

Fig. 22 - Reinforced crimped-free beam

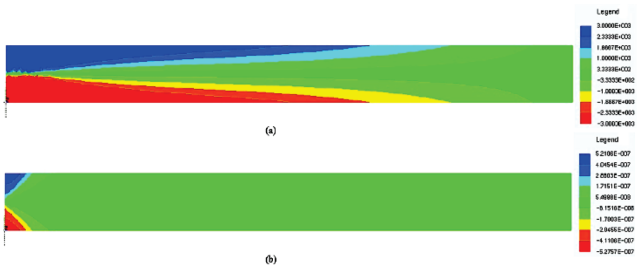

Fig. 23 - (a) tension for the unreinforced structure (b) Plastic deformation for the unreinforced structure

Fig. 24 - (a) tension for the structure with elastic reinforcement (b) Plastic deformation for the structure with elastic reinforcement

400 fiber elements were used to simulate the reinforcement and 476 triangular plate elements for the matrix representation.

Figure 25 shows the graphs of the value of the total reaction as a function of the prescribed vertical displacement for the behavior of elastic fiber and plate, the elastic and elastoplastic plate and the elastoplastic fiber and plate.

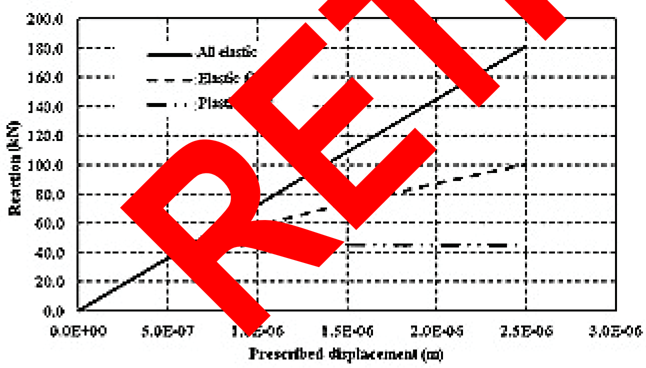

Fig. 25 - Reaction vs. displacement graph

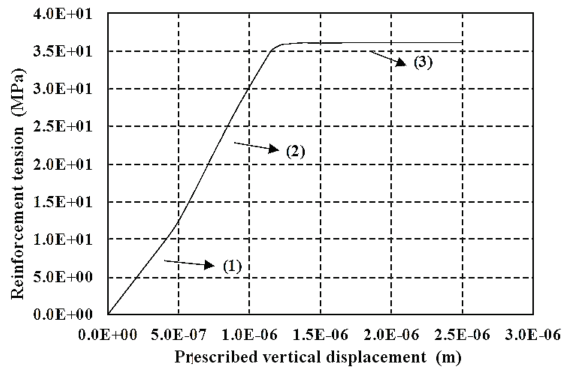

Fig. 26 - Graph of tension in the reinforcement x displacement

Analyzing Figure 25, it is possible to observe that, considering the perfect elastoplastic reinforcement, given the applied displacement, there was also the flow of the reinforcement, since the reaction remained unchanged from approximately one-third of the elastic-elastic displacement applied plastic fiber . As expected, by adopting fiber as elastic, the reaction continues to grow, but at a slower rate than the case with elastic sheet and reinforcement, because the matrix entered the perfect plastic regime, presenting a less rigid system.

Figure 26 shows the tension diagram in the reinforcement next to the crimping as a function of the prescribed vertical displacement adopted.

Analyzing Figure 26, it is possible to observe in section (1) a non-linearity, which occurs by the plastification of the matrix, and not of the material itself. This fact is corroborated by the fact that from this moment, in the section (2), the inclination of the graph with the horizontal increases because there is a greater transfer of effort to the material of the fiber, because when the matrix plastification occurs, it loses stiffness. Only in section (3) does the nonlinearity of the graph occur due to the plastification of the reinforcement itself, adopted as perfect elastoplastic.

These analyzes are carried out only for the purpose of comparing the elastic results of the matrix and the fiber obtained in the present work with results of the technical theory of homogenization of the section.

The homogenization is done with a correction in the inertia of the reinforcement according to the relation between the moduli of elasticity $n = \dfrac{E_{reinfor}}{E_{plate}}$. As the moduli of elasticity of the reinforcement and plate used are, respectively, 2.10^{12} kN/m^2 and 2.10^{11} kN/m^2, we have n = 10.

Calculating the inertia of the reinforcement I_r and the plate I_p, where the reinforcement area is $A_r = 0.03\ m^2$ with unit width and, consequently, height $h = 0.03\ m$:

$$I_r = n\left(\frac{h_r^3 b}{12} + A_r dist^2\right) = 10\left(\frac{0.03^3.1}{12} + 0.03(0.06667)^2\right) = 1.1[illegible].10^{-3}\ m^4$$

$$I_p = \frac{b(2h)^3}{12} = \frac{\infty 1(2.0,2)^3}{12} = 5,333.10^{-3}\ m^4$$

Since these are two reinforcing bars, the homogenized inertia is given by:

$$I_T = I_p + 2I_r = 7,604[illegible].10^{-3}\ m^4$$

According to the theory of the elastic line, the value of the displacement for the free edge according to the elastic line response for the adopted structure is given by $\delta = PL^3/3EI$. The values of displacement in the last step, length of the span, modulus of elasticity and inertia, and realizing the necessary substitutions are known, it is possible to reach a reaction value of *178,23 kN* for the classical solution. Observing Figure 25, it is possible to observe that the result obtained by the code for the reaction value under the same conditions is *180.93* kN, resulting in a relative difference of 1.51% between the values obtained.

Thus, it is possible to verify that the present computational code is coherent with the classical theory, which considers small displacements and linear elastic materials, however, it goes beyond and allows analyzing means reinforcements with physical nonlinearity in both the plate and reinforcement, besides representing correctly structures with large displacements, thus contemplating two different types of non-linearity.

5 Final considerations

The paper has described recent progress on materials modelling and numerical simulation of the phenomenon of physical and geometric nonlinearity in flat reinforced composites with fibers. The work is based on the application of the finite element formulation positional, which has nodal parameters the positions of the nodes and uses a total Lagrangian description for the nonlinear geometric balance. The static equilibrium of the system was obtained by the principle of stationary total potential energy and the resolution of the nonlinear system was obtained by Newton-Raphson's iterative-incremental method.

The constitutive law of Saint-Venant Kirchhoff was adopted, which uses the measure of deformation of Green-Lagrange and the tensor of tensions of Piola-Kirchhoff of second species.

Numerical simulation using the finite element of bar with the insertion of the reinforcement in the medium, whose contribution in the medium is made according to the finite element shape functions of sheet and a compatibilization in the contribution in the degrees of freedom of this, with no increase of degrees of freedom in the system, were compared with analytic formulation gave encouraging results.

The model of plasticity adopted for the matrix was von Mises associative and the solution of the nonlinear equation resulting from its consistency condition was obtained according to iterative solution by the Newton-Raphson method. The model adopted for the fibers, in which the possibility of failure in the fibers or fiber-matrix interface was considered, presented good results, opening possibilities of future analysis.

The efficiency and correct implementation of the adopted formulations can be proven by the several examples shown, in which the obtained results presented values close to the theoretical values and consistent behavior throughout all the analyzes. For the perfect elastoplasticity, the displacement control was more stable in the results and with a lower processing time than the force control.

The computational code developed in the present work allows evaluating different mechanisms involved in reinforcement plasticity, besides correctly representing the plasticity in the plate and the interaction between the two elastoplastic phases. Reinforcement can be considered at random or fixed and aligned.

The positional finite element used has as reference the initial configuration, thus dealing with Lagrangian Total. For the present work, the cubic approximation for the positions was adopted.

Afterwards, the reinforcement code was implemented. The verification of the code was done through comparison with technical solutions (with simplifying hypotheses) of the Resistance of Materials.

Finally plasticity was implemented in both the medium and the fibers. The verification was done by comparing with the Ansys software for the plate metal element. In order to verify fiber plasticity, it was compared with technical solutions, as well as in the implementation phase of the reinforcement itself.

Future developments will, on the one hand, aim at the three-dimensional case that increases the possibility of representations of the most varied structures, the possibility to introduce finite elements that simulate particles and voids, culminating in an increasingly real simulation of the heterogeneous materials, and the implementation of a temporal integrator allowing analysis of problems in which s[illegible] effects are significant to the results. With an eventual use of a temporal integrator, it becomes interesting to parallel[illegible] the [illegible]ed code, since the computational cost spent in these analyzes with consideration of the dynamic behavior will be much larger, when compared to the static cases. On the other hand, the implementation of a damage model would be a matter of extreme importance, since, as previously seen, one of the main functions of fiber use is the control of cracking, in addition to this phenomenon being able to occur simultaneously with plasticity.

REFERENCES

[1]- R.M. Jones, Mechanics of Composite Materials. 2nd Ed. Taylor & Francis, 1999.
[2]- I.M. Daniel, O. Ishai, Engineering Mechanics of Composite Materials. Oxford University Press, Inc. 2006.
[3]- P.K. Mehta, P.J.M. Monteiro, Concrete: microstructure, properties and materials. 3rd Ed. McGraw-Hills Companies, Inc. 2006.
[4]- B. Harris, Engineering Composite Materials. London: The institute of materials. IOM, 1999.
[5]- L. Vanalli, R.R. Paccola, M.R. Scoaris, H.B. Coda, A simple method for non-linear analysis of steel fiber reinforced concrete. Acta Scientiarum-Tech. 32(4) (2010) 367–374. doi:10.4025/actascitechnol.v32i4.7249
[6]- H.M. Gomes, A.M. Awruch, Some aspects on three-dimensional numerical modelling of reinforced concrete structures using the finite element method. Adv. Eng. Softw. 32(4) (2001) 257–277. doi:10.1016/S0965-9978(00)00093-4
[7]- F. Barzegar, S. Maddipudi, Generating reinforcement in fem modelling of concrete structures. J. Struct. Eng-ASCE, 120(5) (1994) 1656–1662. doi:10.1061/(ASCE)0733-9445(1994)120:5(1656)
[8]- J. Bonet, R.D. Wood, J. Mahaney, P. Heywood, Finite element analysis of air supported membrane structures. Comput. Meth. Appl. M. 190(5-7) (2000) 579–595. doi:10.1016/S0045-7825(99)00428-4
[9]- H.B. Coda, An exact FEM geometric non-linear analysis of frames based on position description. In: Proceedings of the 17th international congress of mechanical engineering, São Paulo, Brazil, 2003.
[10]- L. Vanalli, The BEM and FEM applied to the analysis of viscoplastic problems in anisotropic compounds. School of Engineering of São Carlos - University of São Paulo, 2004.
[11]- L. Vanalli, R.R. Paccola, H.B. Coda, A simple way to introduce fibers into FEM models. Commun. Numer. Meth. En. 24(7) (2008) 585–603. doi:10.1002/cnm.983

[12]- R. Hameed, A. Sellier, A. Turatsinze, F. Duprat., Damage model for concrete reinforced with sliding metallic fibers. Int. J. Mech. Mater. Des. 7(1) (2011) 83–97. doi:10.1007/s10999-011-9152-8

[13]- A.S. Khan, S. Huang, Continuum Theory of Plasticity. John Wiley & Sons Ltd, 1995.

[14]- J. Lubliner, Plasticity Theory. Dover Publication Inc. 2008.

[15]- I. Doltsinis, Elements of Plasticity – Theory and Computation. 2. Ed. Southampton, Wessex Institute of Technology Press, WIT Press. 2010.

[16]- S.P.B. Proença, Nonlinear analysis of structures. School of Engineering of São Carlos - University of São Paulo, 2013.

[17]- K. Mattiasson, Numerical results from large deflection beam and frame problems analysed by means of elliptic integrals. Int. J. Numer. Meth. Eng. 17(1) (1981) 145–153.

[18]- G.V. Nogueira, M.S.M. Sampaio, R.R. Paccola, H.B. Coda, Consideration of the slip in the analysis of fiber - reinforced two - dimensional elastic solids using the positional finite element method. In: Proceedings of the XXXV Iberian Latin-American Congress on Computational Methods in Engineering, Fortaleza, CE, Brazil, 2014.